Report no. changed (Mar 2006): SM-373-UU

SACLANTCEN MEMORANDUM
serial no: SM- 373

SACLANT UNDERSEA RESEARCH CENTRE REPORT

On the spatial variability of the impulse response of an underwater acoustic channel

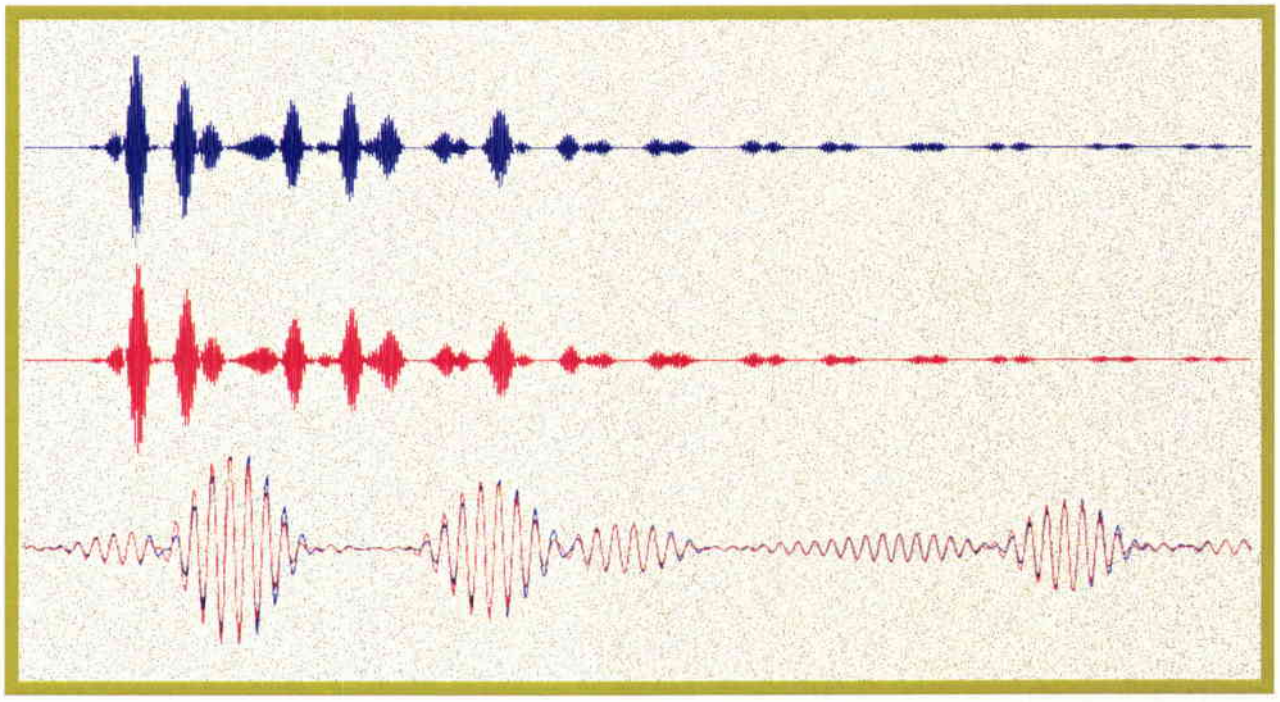

Rolf Weber

May 2000

NORTH ATLANTIC TREATY ORGANIZATION ORGANISATION DU TRAITE DE L'ATLANTIQUE NORD

On the Spatial Variability of the Impulse Response of an Underwater Acoustic Channel

R. Weber

The content of this document pertains to work performed under Project 04-A of the SACLANTCEN Programme of Work. The document has been approved for release by The Director, SACLANTCEN.

Jan L. Spoelstra
Director

intentionally blank page

On the Spatial Variability of the Impulse Response of an Underwater Acoustic Channel

R. Weber

Executive Summary: High-frequency sound propagation in shallow water is highly sensitive to changes in the environmental parameters like water depth, source-receiver range or bottom slope, etc., leading to a high spatial variability of the channel impulse response. Among others, this may influence the performance of adaptive channel equalization techniques for UW communication, focused field concepts, beam-forming, or matched field processing. It is therefore important to understand the effects of these parameter variations on the impulse response and to obtain a quantitative measure of the sensitivity of the impulse response to those parameter changes.

To study this effect, broadband sound propagation (frequency range: 1800 Hz to 2800 Hz) in shallow water is simulated for selected synthetic environments with varying source-receiver geometry and varying bathymetry using a recently developed broadband normal-mode model (PROSIM).

As a measure of similarity between impulse responses two correlators are used. The first one is the classical correlation coefficient which is easy to compute but highly sensitive to a mere time delay between the two functions correlated. As such a time delay usually can be compensated for, the maximum absolute value of the cross correlation function between the complex equivalent lowpass representation of the signals is introduced. The use of the complex lowpass signals is motivated by the fact that the correlation function between the original signals oscillates due to an inherent carrier frequency as their spectrum is not centered around zero thus leading to numerical problems when searching for the maximum.

For the perturbation of the receiver depth and the source-receiver distance, results with both correlators are shown. In the latter case a very high correlation length is obtained with the complex correlator indicating that time delay is the dominant effect. Furthermore, results using the complex correlator with varying water depth and bottom slope are presented. This allows some general remarks on the influence of these parameters.

intentionally blank page

On the Spatial Variability of the Impulse Response of an Underwater Acoustic Channel

R. Weber

Abstract: In many applications like adaptive equalization, beam-forming, matched field processing or focalization the performance is limited due to changes in the impulse response caused by variations in source-receiver range or in bathymetry. As one wishes to quantify the degree of degradation and possibly compensate them it is important to understand the effects of parameter variations on the impulse response.

This report focuses on examining the similarities of simulated impulse responses belonging to scenarios in which environmental parameters are changed one at a time. As a measure of similarity the classical correlation coefficient and the maximum magnitude of the cross correlation function between the complex equivalent lowpass representation of the signals are introduced and their properties are discussed. The results of the correlation analysis demonstrate the properties of the two correlators and show the limits of their applicability. Furthermore, they give evidence that some parameter perturbations are more critical for impulse response variations than others.

Keywords: Correlation Analysis ∘ Impulse Response Variations ∘ Sound Propagation Modelling

Contents

1 Introduction

High-frequency sound propagation in shallow water is highly sensitive to changes in the environmental parameters like water depth, source-receiver range or bottom slope leading to changes in the impulse response of the underwater acoustic sound channel. These spatial impulse response variations may cause a reduction in performance of acoustic underwater communication systems and sonar systems which shall be demonstrated by an examples.
Consider an *adaptive equalizer* for underwater digital communication systems and assume for example a ship with a towed source moving slowly enough so that Doppler effects and timing problems can be compensated at the receiver prior to equalization. Then, because of the changing source-receiver geometry due to the movement and the possibly changing boundary conditions there will occur variations in the impulse response to be equalized. To perform equalization it is necessary for the adaptive algorithm to converge before the impulse response changes considerably. Furthermore, tracking of the channel parameters is only possible in the case of slow variations [12]. Therefore, it is necessary to know which influence on the impulse response changes in certain parameters cause and how rapidly transmission conditions change with these environmental parameters.
Further applications for correlation analysis of underwater acoustic channel impulse responses may include *beam-forming*, [15], *matched field processing*, [1, 22], and *focalization*, [8, 10].

To study the effects of parameter changes, underwater acoustic sound propagation is *simulated* using a broadband normal-mode model together with realistic channel properties. This allows us to easily change the source-receiver geometry and the bathymetry independently and examine their influence on the impulse response. For a first approach and to obtain some general insight effects like ambient noise, a range-dependent sound-speed profile, surface wave motion and internal waves are not taken into account.
The *spatial correlation* between two impulse responses is used to measure mutual relationships existing between these functions. The easy to compute classical *correlation coefficient* [5]

$$\rho_{12} = \frac{\int_{-\infty}^{\infty} p_1(t)\, p_2^*(t)\, \mathrm{d}t}{\sqrt{\int_{-\infty}^{\infty} |p_1(t)|^2\, \mathrm{d}t \cdot \int_{-\infty}^{\infty} |p_2(t)|^2\, \mathrm{d}t}}$$

between two functions p_1 and p_2 is introduced as a first approach.

However, it will become evident that one essential drawback of the correlation coefficient is its sensitivity to mere time delays between the functions to be correlated. This leads to extremely small values of the correlation at a time delay corresponding to a distance of a fraction of the wavelength only. To circumvent this problem the *maximum absolute value of the cross correlation function* between the complex equivalent lowpass representations of the signals will be introduced as a correlator. Then, this correlator will be used to measure the similarities between simulated impulse responses when the source-receiver distance, the water depth or the bottom slope are gradually changed. The results of this analysis show that the latter two parameters are far more critical for impulse response variations than the first one.

This report is organized as follows:
Section 2 presents the necessary physical background material. First, a short derivation of the linear acoustic wave equation is given followed by a normal-mode approach to its solution. Then, Fourier synthesis of frequency-domain solutions is introduced. **Section 3** is denoted to correlation analysis. The classical correlation coefficient is derived and its advantages as well as its disadvantages are discussed. The disadvantages lead to the introduction of the complex correlation coefficient. The performed simulations with both correlators are also described in this section and their results are discussed. In **Section 4** the results are summarized and some further conclusions are drawn. Additionally, some suggestions for further work are made. This report is completed by some acknowledgements in **Section 5**, the used **References** and some derivations concerned with the complex baseband equivalent signals in **Annex A**.

2

Acoustic Propagation Model

2.1 Normal-Mode Solution of the Linear Acoustic Wave Equation

Let $p(\mathbf{r},t)$ denote the pressure field within a fluid as a function of space *mathbfr* and time t. The equilibrium density of the medium is given by $\rho_0(\mathbf{r})$ and the speed of sound by $c(\mathbf{r})$. Then, the *linear wave equation for the pressure field* is given by [4]

$$\rho_0(\mathbf{r})\nabla\left(\frac{1}{\rho_0(\mathbf{r})}\nabla p(\mathbf{r},t)\right) - \frac{1}{c(\mathbf{r})^2}\frac{\partial^2 p(\mathbf{r},t)}{\partial t^2} = f(\mathbf{r},t)\,, \tag{1}$$

where $f(\mathbf{r},t)$ represents the driving force as a function of space and time. To solve Eq. (1) proper boundary conditions describing the pressure field at the interfaces of different media are also necessary.

Note that the coefficients of the two differential operators in equation (1) are independent of time. Therefore, applying the *Fourier transformation*, given by the identities

$$f(\omega) = \int_{-\infty}^{\infty} f(t)\,\mathrm{e}^{i\omega t}\mathrm{d}t$$

$$f(t) = \frac{1}{2\pi}\int_{-\infty}^{\infty} f(\omega)\,\mathrm{e}^{-i\omega t}\mathrm{d}\omega\,,$$

reduces the dimension of the wave equation to three:

$$\rho_0(\mathbf{r})\nabla\left(\frac{1}{\rho_0(\mathbf{r})}\nabla p(\mathbf{r},\omega)\right) + k^2(\mathbf{r})\,p(\mathbf{r},t) = f(\mathbf{r},\omega)\,, \tag{2}$$

where $k(\mathbf{r})$ is the *medium wavenumber* at radial frequency ω, given by

$$k(\mathbf{r}) = \frac{\omega}{c(\mathbf{r})}\,.$$

Although the *frequency-domain Helmholtz equation* (2) is easier to solve than the original differential equation (1), the desired solution $p(\mathbf{r},t)$ is obtained from $p(\mathbf{r},\omega)$ only after solving a Fourier integral.

The approach is now as follows: possibly *range-dependent* environments are divided into a number of segments in which the acoustic field is approximated as range independent. In each such segment the standard normal-mode solution for the corresponding frequency-domain Helmholtz equation (2) together with proper interface conditions is calculated [9]. To reduce the computational complexity the segments are coupled by applying the adiabatic approximation which assumes no energy transfer to higher or lower modes when going from one range to the next [13].
The resulting complex pressure field in cylindrical coordinates for a *point source* at depth z_S excited by a time-domain impulse is then given by

$$p(r,z,\omega) \approx \frac{i}{\rho_0(z_S)\sqrt{8\pi}}\,\mathrm{e}^{-i\pi/4}\sum_{m=1}^{\infty}\Psi_m(0,z_S)\,\Psi_m(r,z)\,\frac{\mathrm{e}^{i\int_0^r k_{rm}(r',\omega)\,dr'}}{\sqrt{\int_0^r k_{rm}(r',\omega)\,dr'}}\,. \tag{3}$$

At any range r, k_{rm} are the eigenvalues and Ψ_m the eigenfunctions (modes) of the Sturm-Liouville problem [4] obtained by a separation of variables approach to solve Eq. (2).

The calculation of the *spatial transfer function* $p(r,z,\omega)$ is performed by the recently developed simulation tool PROSIM [19].

2.2 Broadband Modeling

The normal-mode solution to the wave equation delivers the spatial transfer function $p(r,z,\omega)$. Denoting the source spectrum by $S(\omega)$, the time-domain solution $p(r,z,t)$ can be found via an inverse Fourier transform of the product of the two spectra [18]:

$$p(r,z,t) = \frac{1}{2\pi}\int_{-\omega_{\max}}^{\omega_{\max}} S(\omega)\,p(r,z,\omega)\,\mathrm{e}^{-i\omega t}\mathrm{d}\omega\,. \tag{4}$$

In Eq. (4) it is further assumed that the source does not significantly emit energy above a certain radial frequency $\omega_{\max}$.
To calculate the integral in equation (4) efficiently, a time observation window of length T, starting at $t_{\min}$, is introduced and both time and frequency axes are discretized

$$t_m = t_{\min} + m\Delta t\,, \qquad 0 \le m < N\,,$$
$$\omega_n = n\Delta\omega\,, \qquad -(N/2) < n \le (N/2)\,,$$

such that the time and frequency samples fulfill the relationship

$$\Delta t\Delta\omega = \frac{2\pi}{N} \tag{5}$$

and N is supposed to be a power of 2. Then, the Fourier-integral can be efficiently computed using a *Fast-Fourier-Transform algorithm* (FFT) at each spatial position (r,z). For a proper approximation, we clearly have to satisfy the condition

$(N/2)\,\Delta\omega \geq w_{\max}$ which - together with equation (5) - guarantees that *Shannon's sampling theorem*

$$f_S := \frac{1}{\Delta t} \geq 2\, f_{\max}$$

is fulfilled [18].
It is well known that sampling in frequency leads to a time signal which is periodic with period $T = N\Delta t$, [17]:

$$\sum_{l=-\infty}^{\infty} p(r, z, t_{\min} + t_m + lT)\,.$$

Therefore, the length T of the observation window must be chosen long enough to contain all the signal energy except for a negligible small amount. In that case no aliasing occurs and we can separate one period of the above signal which closely approximates the original time function.
Then, approximating the integral in (4) by using the rectangle-rule and sampling the time and frequency axes like introduced above yields:

$$p(r, z, t_{\min} + t_m) = \frac{\Delta\omega}{2\pi} \sum_{n=-(N/2-1)}^{N/2} P(r, z, \omega_n)\, W_N^{-nm}\,,$$

where the abbreviations

$$P(r, z, \omega_n) := S(\omega_n)\, p(r, z, \omega_n)\, \mathrm{e}^{-i\omega_n t_{\min}}\,, \qquad -(N/2) < n \leq (N/2)\,, \tag{6}$$

and

$$W_N := \mathrm{e}^{i2\pi/N}$$

are used. Re-arranging the N frequency samples in equation (6) like follows

$$\tilde{P}(r, z, \omega_n) = \begin{cases} P(r, z, \omega_n) & ,0 \leq n \leq N/2 \\ P(r, z, \omega_{n-N}) & ,N/2+1 \leq n < N \\ 0 & ,\text{otherwise} \end{cases}\,,$$

and observing that the values of W_N^{-n} are equally spaced on the unit circle, we obtain

$$\begin{aligned} p(r, z, t_{\min} + t_m) &= \frac{\Delta\omega}{2\pi} \sum_{n=0}^{N-1} \tilde{P}(r, z, \omega_n)\, W_N^{-nm} \\ &= \Delta t \cdot \mathrm{IDFT}\left\{\tilde{P}(r, z, \omega_n)\right\}\,, \end{aligned}$$

where we used equation (5) and IDFT denotes the inverse discrete Fourier transform of a sequence [17].

3

Correlation Analysis of Impulse Responses

Correlation is the act of processing two deterministic signals to determine mutual relationships between some of their important characteristics like shape or relative delay. The concept of correlation is widely used in receivers for digital communications [16] and sonar [24].

3.1 The Classical Correlation Coefficient

Let $\mathcal{L}^2(\mathbb{C})$ denote the *Hilbert space* of square integrable functions (energy signals) equipped with the inner product

$$< p_1, p_2 >= \int_{-\infty}^{\infty} p_1(t) p_2^*(t)\, \mathrm{d}t\,,$$

where $p_1, p_2 \in \mathcal{L}^2(\mathbb{C})$. If we now want to determine a quantitative measure of the degree to which p_1 and p_2 are "alike" we form the unit-norm vectors $p_1/||p_1||$ and $p_2/||p_2||$, where the norm is given by

$$||p|| := \sqrt{< p, p >}\,,$$

and *orthogonally project* one of these vectors on the other:

$$\mathrm{P}\left(\frac{p_1}{||p_1||}, \frac{p_2}{||p_2||}\right) = \left\langle \frac{p_1}{||p_1||}, \frac{p_2}{||p_2||} \right\rangle \cdot \frac{p_1}{||p_1||} = \underbrace{\left(\frac{< p_1, p_2 >}{||p_1||\,||p_2||}\right)}_{=:\rho_{12}} \cdot \frac{p_1}{||p_1||}\,,$$

where $\mathrm{P}(a, b)$, $a, b \in \mathcal{L}(\mathbb{R})$, denotes the *projector* of b onto a. The factor

$$\rho_{12} = \frac{< p_1, p_2 >}{||p_1||\,||p_2||} = \frac{\int_{-\infty}^{\infty} p_1(t)\, p_2^*(t)\, \mathrm{d}t}{\sqrt{\int_{-\infty}^{\infty} |p_1(t)|^2\, \mathrm{d}t \cdot \int_{-\infty}^{\infty} |p_2(t)|^2\, \mathrm{d}t}} \tag{7}$$

is called the *normalized correlation coefficient* as its values are in the range $[-1; 1]$. A frequency domain expression for the correlation coefficient (7) can be found by using Parseval's identity [18]

$$\int_{-\infty}^{\infty} p_1(t) p_2^*(t)\, \mathrm{d}t = \frac{1}{2\pi} \int_{-\infty}^{\infty} p_1(\omega) p_2^*(\omega)\, \mathrm{d}\omega\,,$$

where $p_1(\omega)$, $p_2(\omega)$ are the Fourier transforms of $p_1(t)$ and $p_2(t)$ respectively, leading to

$$\rho_{12} = \frac{\int_{-\infty}^{\infty} p_1(\omega)\, p_2^*(\omega)\, \mathrm{d}\omega}{\sqrt{\int_{-\infty}^{\infty} |p_1(\omega)|^2\, \mathrm{d}\omega \cdot \int_{-\infty}^{\infty} |p_2(\omega)|^2\, \mathrm{d}\omega}} \tag{8}$$

The magnitude of the correlation coefficient will be close to one if the two functions are similar and it will be zero when they are orthogonal to each other which means that they are dislike the most. Therefore, the magnitude of the correlation coefficient as given either in (7) or (8) is chosen as a measure of similarity between two functions. In order to compute the correlation coefficient for discrete-time data the integrals in equations (7) and (8) are approximated using the rectangle-rule yielding

$$\begin{aligned} \rho_{12} &= \frac{\sum_{k=-\infty}^{\infty} p_1(k\Delta t)\, p_2^*(k\Delta t)}{\sqrt{\sum_{k=-\infty}^{\infty} |p_1(k\Delta t)|^2 \cdot \sum_{k=-\infty}^{\infty} |p_2(k\Delta t)|^2}} \\ &= \frac{\sum_{\nu=-\infty}^{\infty} p_1(\nu\Delta\omega)\, p_2^*(\nu\Delta\omega)}{\sqrt{\sum_{\nu=-\infty}^{\infty} |p_1(\nu\Delta\omega)|^2 \cdot \sum_{\nu=-\infty}^{\infty} |p_2(\nu\Delta\omega)|^2}}. \end{aligned} \tag{9}$$

3.2 Examples

For a first survey we assume a range-independent three layer scenario. The environmental parameters are listed in Table 1 and the sound speed profile for the single layers is depicted in Fig. 1.

	depth [m]	density (rel. to water)	attenuation [dB/λ]
water column	120	1	0
sediment	10	1.2	1
sub-bottom	∞	2	0.8

Table 1 *Environmental parameters for range-independent scenario.*

The used sound-speed profile in the water column is a measured downward refracting shallow-water sound-speed profile acquired in May. The parameters for the sediment layer and the sub-bottom have been chosen as typical values for silt and sand, respectively [13].

As common underwater digital communication or sonar systems are typically bandlimited we restrict the computation of the transfer function to a bandwidth of $B = 1\,\mathrm{kHz}$, centered around the carrier frequency $f_c = 2300\,\mathrm{Hz}$. In order to suppress sidelobes due to the now inherent frequency-domain filtering a Hanning window

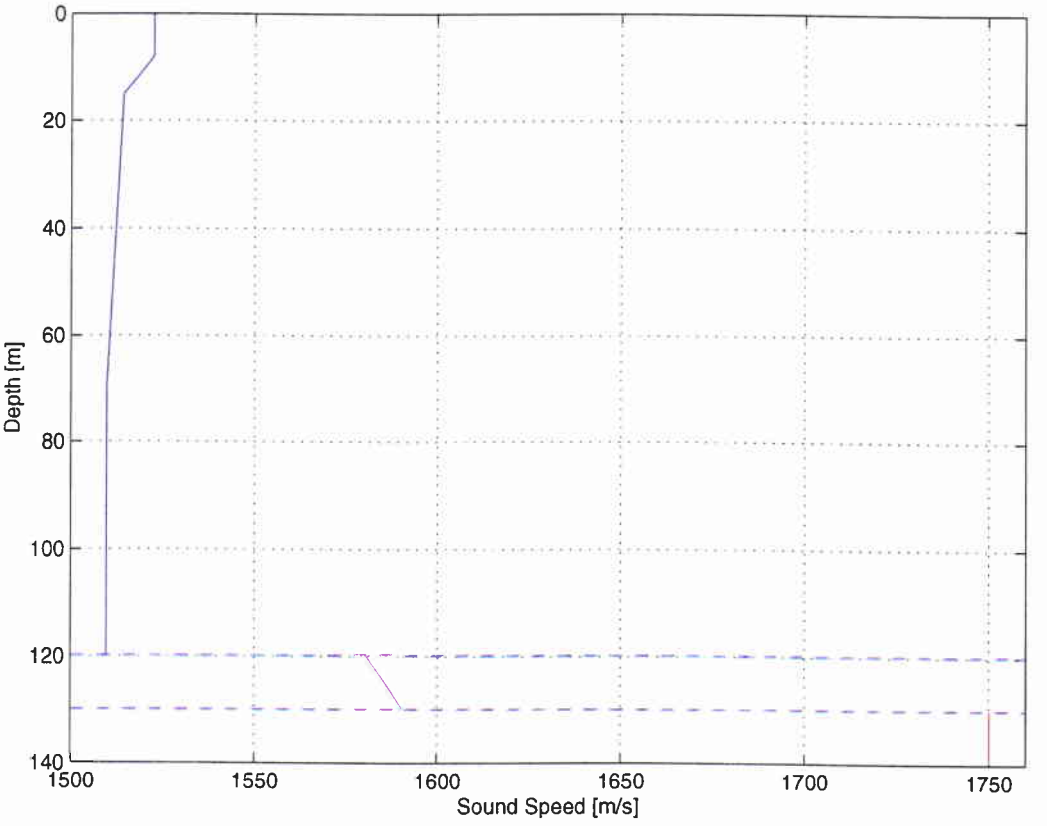

Figure 1 *Sound speed profile in the water column, sediment layer and sub-bottom halfspace as function of depth.*

instead of a simple rectangular window is used[1] reducing the sidelobes by approximately 20 dB at the cost of doubling the width of the main lobe [17].

Case 1: Depth varying receivers

The omnidirectional source is placed at a water depth of 60 m. The receiver is positioned 20 km downrange and varies in depth. Fig. 2 shows the resulting impulse responses at various depths.

It can be clearly seen that the obvious characteristics of the impulse responses like occurrence of direct arrivals and their strength as well as the number of reverberations and the thereof resulting time spread considerably change with depth.

Now, the hydrophone at a depth of 60 m is arbitrarily chosen as a reference and the correlation coefficient ρ_{12} between this particular impulse response and those for depth variations is computed. The result is shown in Fig. 3.

It can be seen that the function plotted in Fig. 3 is not symmetric with respect to

[1] This leads to an effective bandwidth smaller than B.

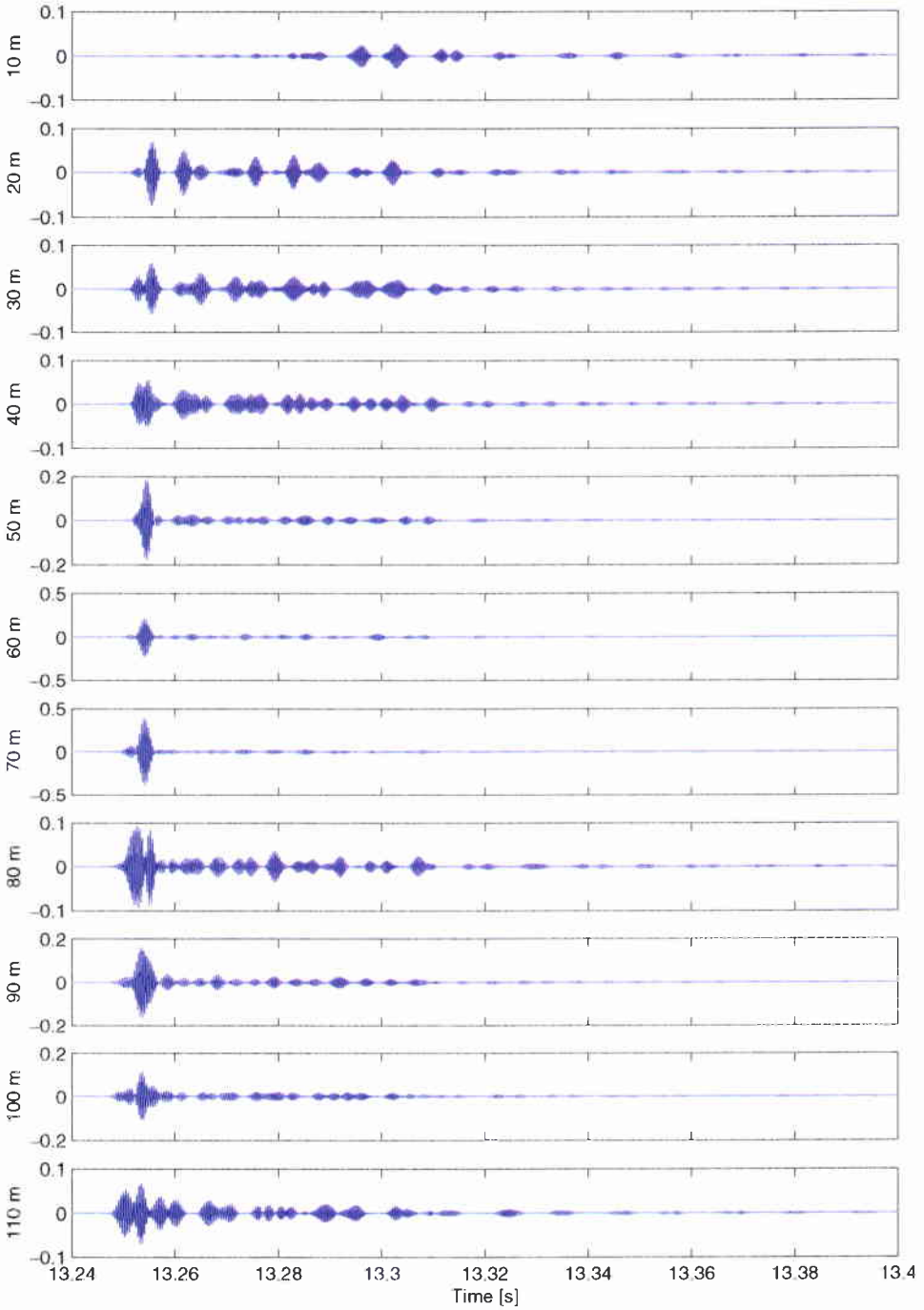

Figure 2 *Impulse responses at a range of 20 km at various depths.*

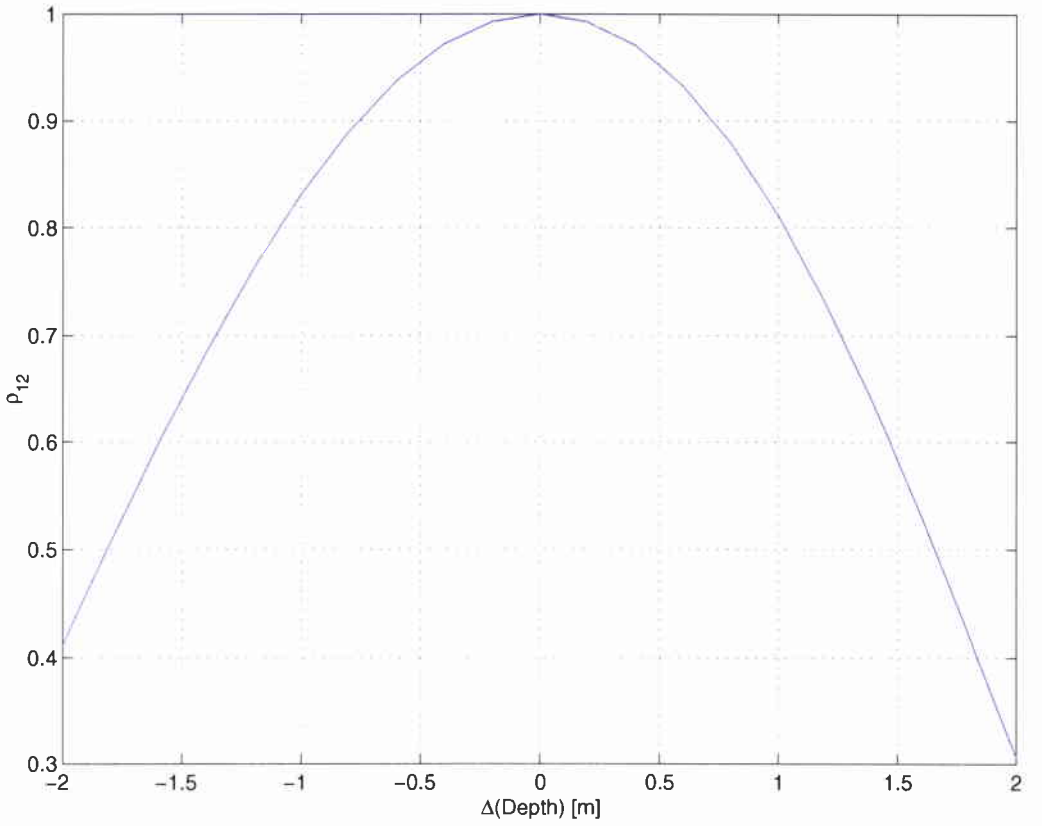

Figure 3 *Correlation coefficient ρ_{12} as a function of receiver depth relative to the hydrophone at a depth of 60 m. The range between transmitter and receivers is 20 km.*

the axis at $\Delta(\text{Depth}) = 0$. This is not surprising taking the unsymmetric propagation behaviour due to the non-constant sound-speed profile, the non-symmetric source-receiver geometry and the boundary conditions into account.
One may consider two impulse responses to be uncorrelated if the correlation coefficient between them decreases by more than 3 dB which means that in this example the two functions would be decorrelated after a relative receiver-depth change of approximately ± 1.3 m. Using as a measure the point where the correlation coefficient drops below a value 0.5 instead leads to a correlation length of approximately ± 1.7 m.
Assuming a vertical receiver array the above statement means that in our special scenario the measured impulse responses at hydrophones more than 1.7 m apart are completely uncorrelated with each other.

Case 2: Range varying receivers
The transmitter is again supposed to be at a water depth of 60 m. The receiver is

20 km away at a depth of 20 m varying in distance now. Using the hydrophone at 20 km as a reference, computation of the correlation coefficient as defined in equation (9) leads to a rapid decay. For example after moving out half a meter in distance the correlation coefficient is down to $\rho_{12} = 0.03$ indicating no similarity between the two functions any more.

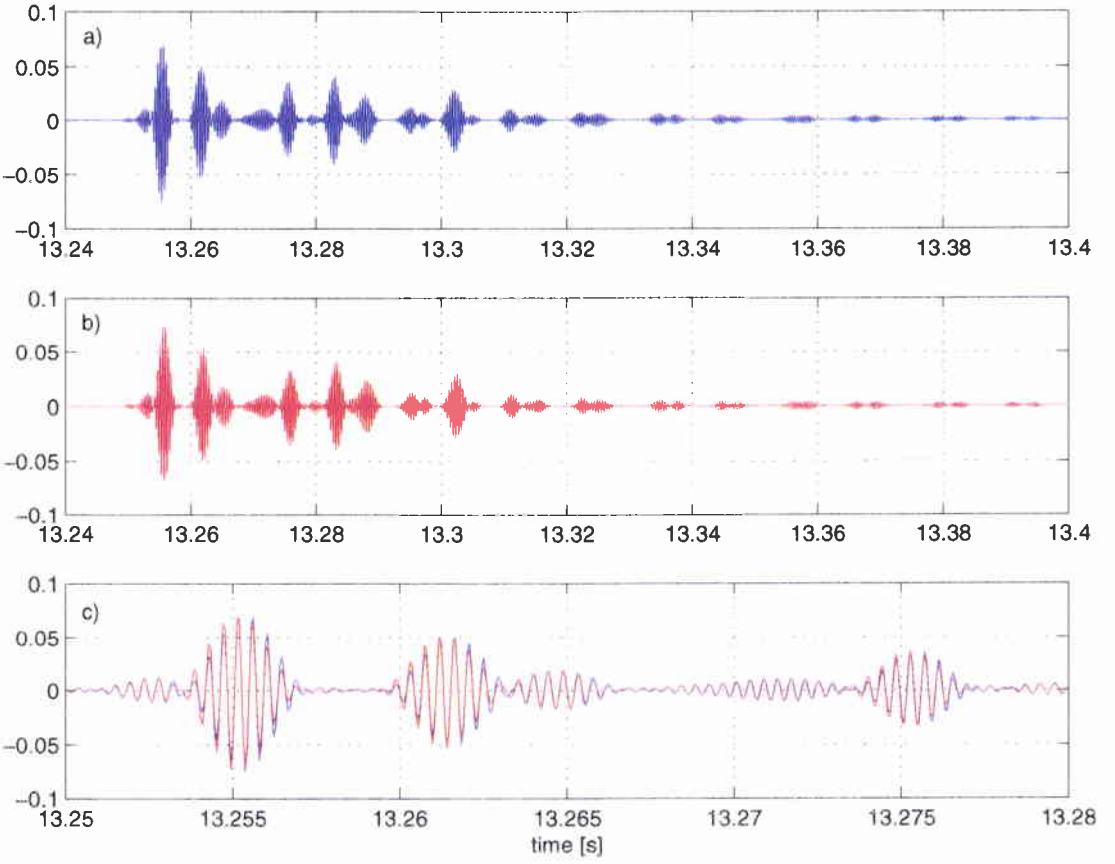

Figure 4 *a) Impulse response at a water depth of 20 m and a range of 20 km. b) Impulse response at a water depth of 20 m and a range of 20.0005 km. c) Both impulse responses after delay time correction.*

The two impulse responses are depicted in Fig. 4 and it can be observed by inspection that apart from a mere time delay the two functions look similar. Correcting this time delay as it is shown in part c) of the figure proofs the high similarity in the shape of the two impulse responses. Correspondingly, calculating the correlation coefficient of the two time delay corrected time series one obtains a value of 0.98 which is sufficiently close to one.

It can be concluded that the correlator defined in equation (9) is very sensitive to time delays larger than those corresponding to a small fraction of the wavelength

λ. As the maximum frequency used is 2800 Hz and the speed of sound in the water column is around 1500 m/s, an approximate value of the wavelength is 0.54 m which is in the range of the hydrophone displacement valid in the experiment. Therefore, the low number of the correlation coefficient can be expected.
In some applications, however, a mere time delay between the signals is not taken into account or it is estimated and/or corrected before further processing. In that case a different definition of the correlation coefficient should be used which is introduced in the next section.

3.3 A Correlator Insensitive to Time Shifts

Let us first revisit the definition of the correlation coefficient given in equation (7). The numerator can be rewritten as

$$\int_{-\infty}^{\infty} p_1(t)\, p_2^*(t)\, \mathrm{d}t = \int_{-\infty}^{\infty} p_1(t)\, p_2^*(t-\tau)\, \mathrm{d}t \Bigg|_{\tau=0} = p_1(\tau) * p_2^*(-\tau)|_{\tau=0} \,,$$

where the asterisk denotes convolution of the two signals p_1 and p_2, see [17]. Allowing τ to be any real number one obtains the *cross-correlation function*

$$R_{12}(\tau) = \int_{-\infty}^{\infty} p_1(t)\, p_2^*(t-\tau)\, \mathrm{d}t$$

which reduces to the *auto-correlation function* $R_{11}(\tau)$ in the case that both signals are identical. The auto-correlation function exhibits conjugate symmetry, $R_{11}(\tau) = R_{11}^*(-\tau)$ and attains its maximum value $||p_1(t)||^2$ at τ equal to zero.
Now, assuming that p_2 is identical to p_1 except for a time delay τ_0, the maximum of the cross-correlation function will again be $||p_1(t)||^2$ and it will be located at $\tau = -\tau_0$. Therefore, searching for the maximum of the cross-correlation function gives the time delay between otherwise identical signals. This is a property widely used in sonar for bearing and range detection of targets [5, 24].
Conversely, defining

$$\rho_{12} := \operatorname{sign}\left(R_{12}(\tau_0)\right) \frac{|R_{12}(\tau_0)|}{||p_1||\,||p_2||} \tag{10}$$

with

$$\tau_0 = \arg\max_{\tau} |R_{12}(\tau_0)|$$

and sign(∘) being the signum of the real-valued expression in parentheses we obtain a correlator that is insensitive to time shifts.
Unfortunately, definition (10) of the correlation coefficient leads to numerical instabilities when performing the maximum search. This is due to the fact that the cross-correlation function essentially oscillates with the carrier frequency of the two functions involved, see equation (13) in Annex A, leading to two problems:

1. Because of the underlying oscillation of the cross-correlation function the sign corresponding to the maximum absolute value of this function can switch from one computation to the next dependent on the carrier frequency without changing the observed parameter considerably. This leads to a non-continuous graph for the correlation coefficient.

2. Therefore, one should rather look for the maximum of the envelope of the correlation function as it is slowly varying compared to the underlying oscillation. But the carrier frequency is not high enough to give smooth samples of the envelope by simply taking the absolute value of the cross-correlation function. This leads to a non-continuous curve for the correlation coefficient because the true maximum cannot be found.

To circumvent these problems we suggest the calculation of the *complex baseband representation* of the original bandpass signals, see Annex A, to become independent of the chosen carrier frequency[2].
Then, if we denote with $\tilde{p}_1$ and $\tilde{p}_2$ the complex baseband representations of p_1 and p_2 respectively, the baseband cross-correlation function is

$$\tilde{R}_{12}(\tau) = \tilde{p}_1(\tau) * \tilde{p}_2^*(-\tau)$$

whose magnitude is maximized for a value

$$\tau_0 = \arg\max_{\tau} |\tilde{R}_{12}(\tau)| .$$

With these quantities the *complex correlation coefficient* $\tilde{\rho}_{12}$ can be defined as follows:

$$\tilde{\rho}_{12} = \frac{|\tilde{R}_{12}(\tau_0)|}{||\tilde{p}_1||\,||\tilde{p}_2||}\, e^{j \arg\{\tilde{R}_{12}(\tau_0)\}} , \tag{11}$$

where arg{o} denotes the phase of the complex argument. Its magnitude is then in the range between zero and one and can be used as a measure of similarity between the two functions considered.

3.4 Examples

The environmental parameters of Table 1 and the sound speed profile of Fig. 1 are again used in the PROSIM simulator to conduct all the simulations which are to be described in the following.

Case 3: Range varying receivers
The setting is the same as for Experiment 2 in Section 3.2: the transmitter is located

[2] As some physical properties of the medium like attenuation are also frequency dependent, the resulting baseband signal is not completely independent of the carrier frequency.

at a water depth of 60 m and the receiver is at a depth of 20 m originally 20 km downrange. Then the distance between source and receiver is gradually changed, with the 20 km being the reference position.
After transforming the obtained impulse responses into their complex baseband representations the correlation coefficient is computed according to equation (11). The magnitude of this quantity is shown in Fig. 5.

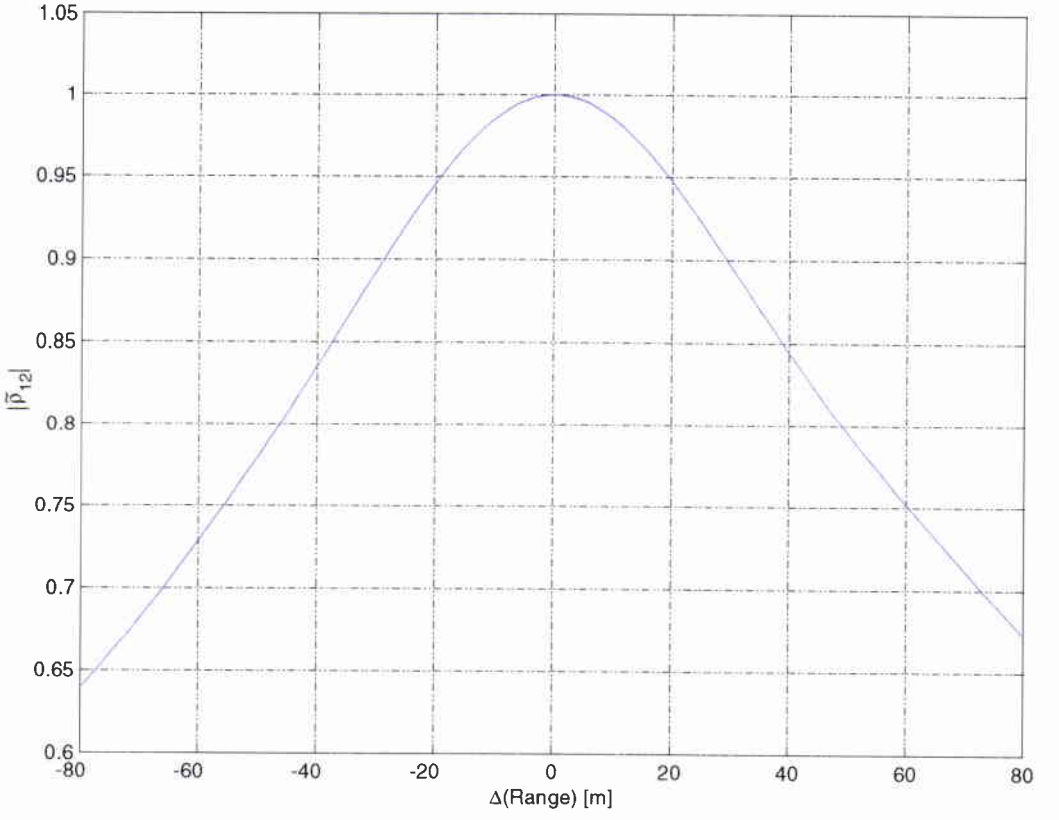

Figure 5 *Magnitude of the complex correlation coefficient $\tilde{\rho}_{12}$ as a function of source receiver distance relative to the hydrophone at a distance of 20 km. The source depth is 60 m and the receiver depth is 20 m.*

Using the point where $|\tilde{\rho}_{12}|$ decreases by 3 dB as a measure of decorrelation the distance between the source and the receiver could vary by approximately ±65 m leading still to sufficient correlation between the impulse responses. Taking values of $|\tilde{\rho}_{12}|$ down to 0.5 into account a correlation length of more than 100 m could be reached.
This correlation length is very high compared to the one obtained in Experiment 2 demonstrating the high similarity between impulse responses over a wide range of the parameter Δ(Range) if a mere time delay is not taken into account. The reason for this behavior is that at an original distance of 20 km most of the energy arriving

at the receiver is conveyed via paths that show no or only very few bottom or surface bounces while other paths with more reflections die out because of losses. Therefore, varying the distance between source and receiver by a small amount essentially leads to an additional delay which is corrected for by the used correlator. This is validated by plots of the impulse responses for various ranges in Fig. 6.

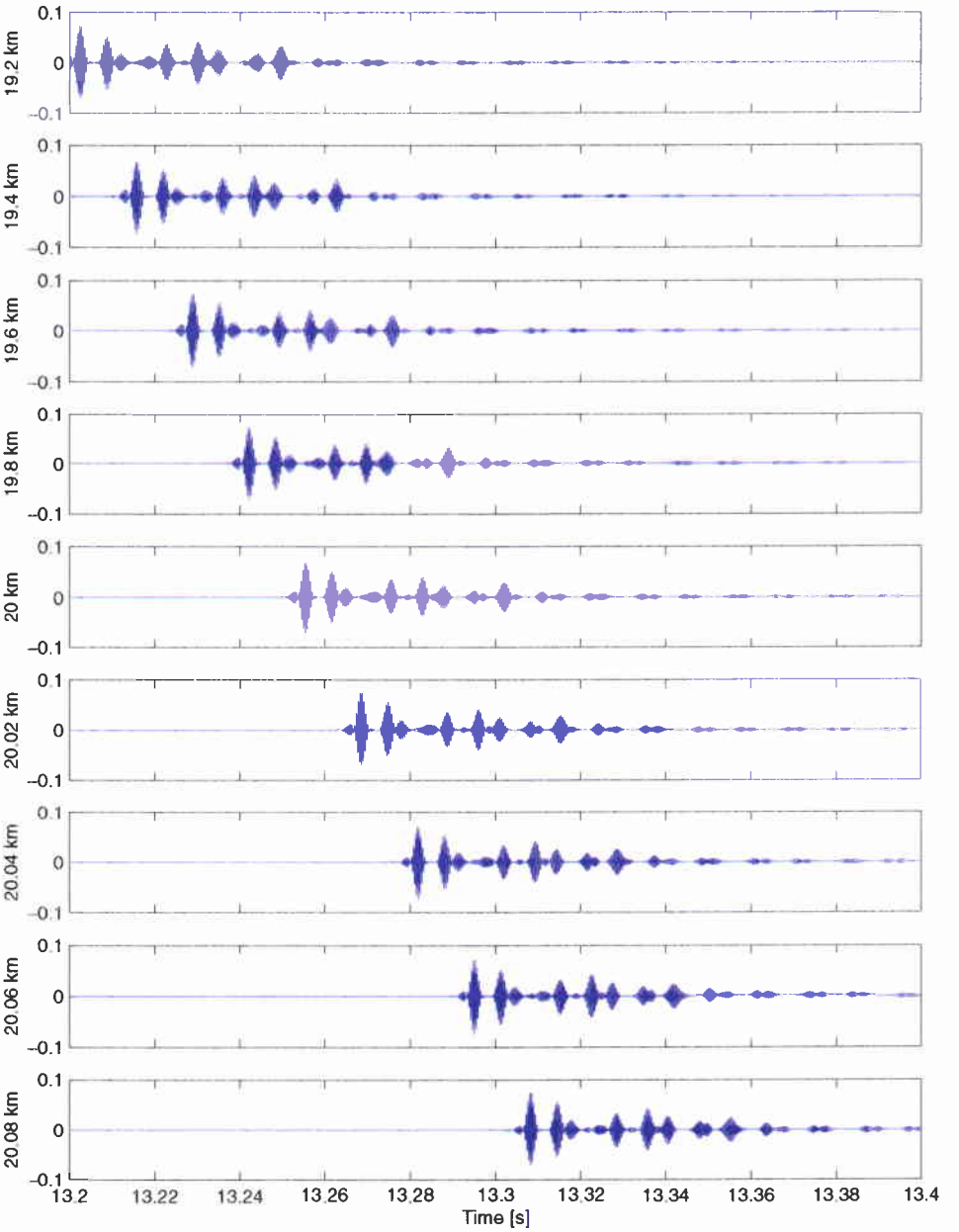

Figure 6 *Impulse responses at 20 m receiver depth at various distances.*

For our the communication receiver example the correlation length imposes a limit on the allowed speed of the moving source if the convergence rate of the used adaptive algorithms is given or vice versa. If delay estimation is possible prior to further processing these restrictions can be greatly relaxed for range varying receivers as comparison of the results of Cases 2 and 2 demonstrates.

Case 4: Varying water depth

The experimental setting is again the one where the transmitter is located at a water depth of 60 m and the receiver is at a depth of 20 m, 20 km away from the transmitter. Now, the original water depth of 120 m is perturbed.

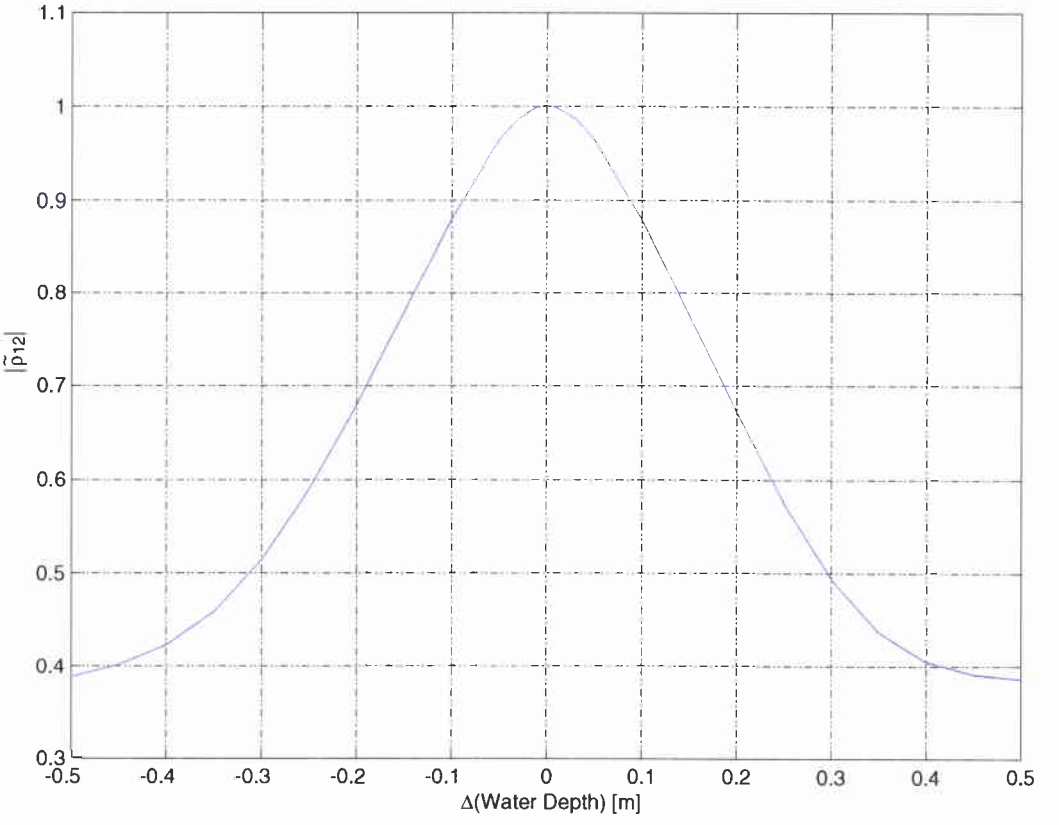

Figure 7 *Magnitude of the complex correlation coefficient $\tilde{\rho}_{12}$ as a function of water depth. The source depth is 60 m, the receiver depth is 20 m and the reference water depth is 120 m.*

The magnitude of the resulting complex correlation coefficient as a function of water depth is then shown in Fig. 7. It is obvious that correlation is obtained only over a very small range of the parameter Δ(Water Depth) (approximately ± 0.2 m when using the 3 dB point) compared to Case 3.

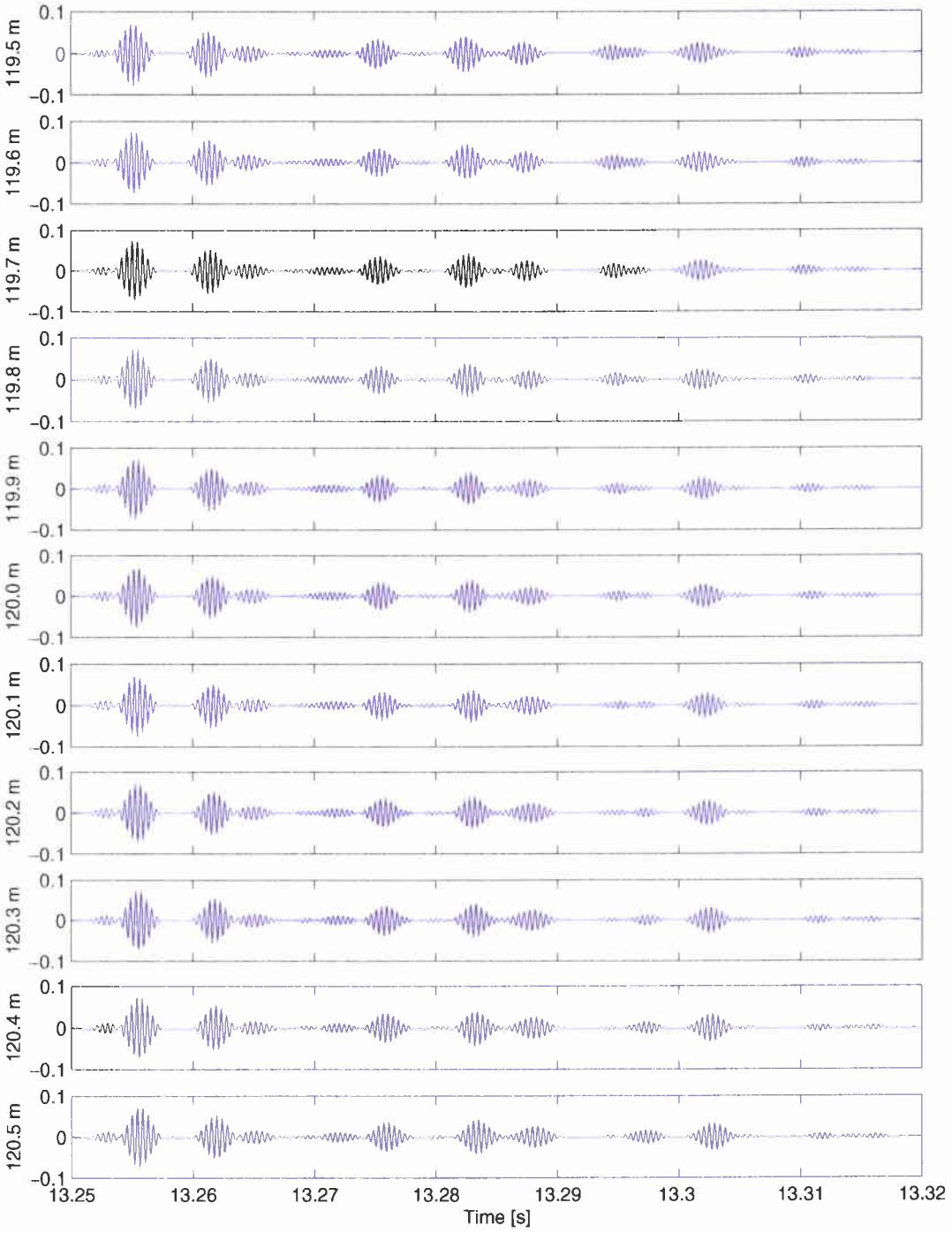

Figure 8 *Impulse responses at a range of 20 km at various water depths.*

This indicates that a change in water depth is a far more sensitive parameter for impulse response variations than a change in the source-receiver distance. The explanation for this behavior is that now distinct portions of the impulse response corresponding to different numbers of surface and bottom reflections show slightly different delays due to the change in water depth and the thereof resulting longer travel time, see Fig. 8. Hence, there is no single delay value between the two functions to be correlated so that less cross-energy is added up leading to a faster decrease in correlation.
The implications on our communication example are twofold. First, there is no single delay to be compensated and second, moving the source through a changing water column leads to faster impulse response variations than in Case 3. This implies the need for faster adapting algorithms if the speed of the source is given even if a time-delay-compensation takes place.

Case 5: Varying bottom slope
Again, the source-receiver geometry is the same as in the previous simulations.

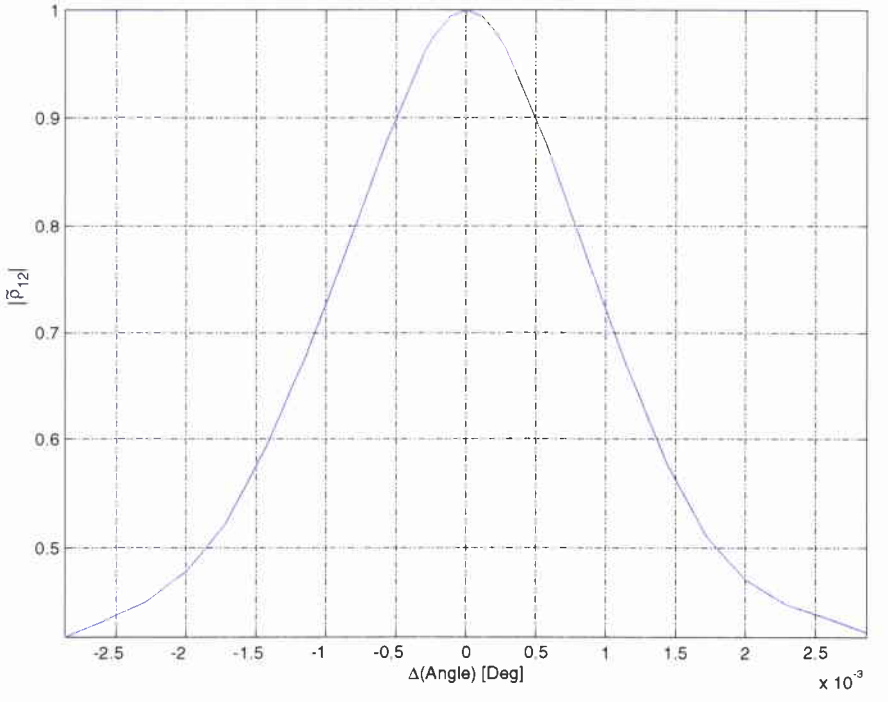

Figure 9 *Magnitude of the complex correlation coefficient $\tilde{\rho}_{12}$ as a function of bottom angle. The source depth is 60 m, the receiver depth is 20 m and the reference water depth at an angle of zero degree is 120 m.*

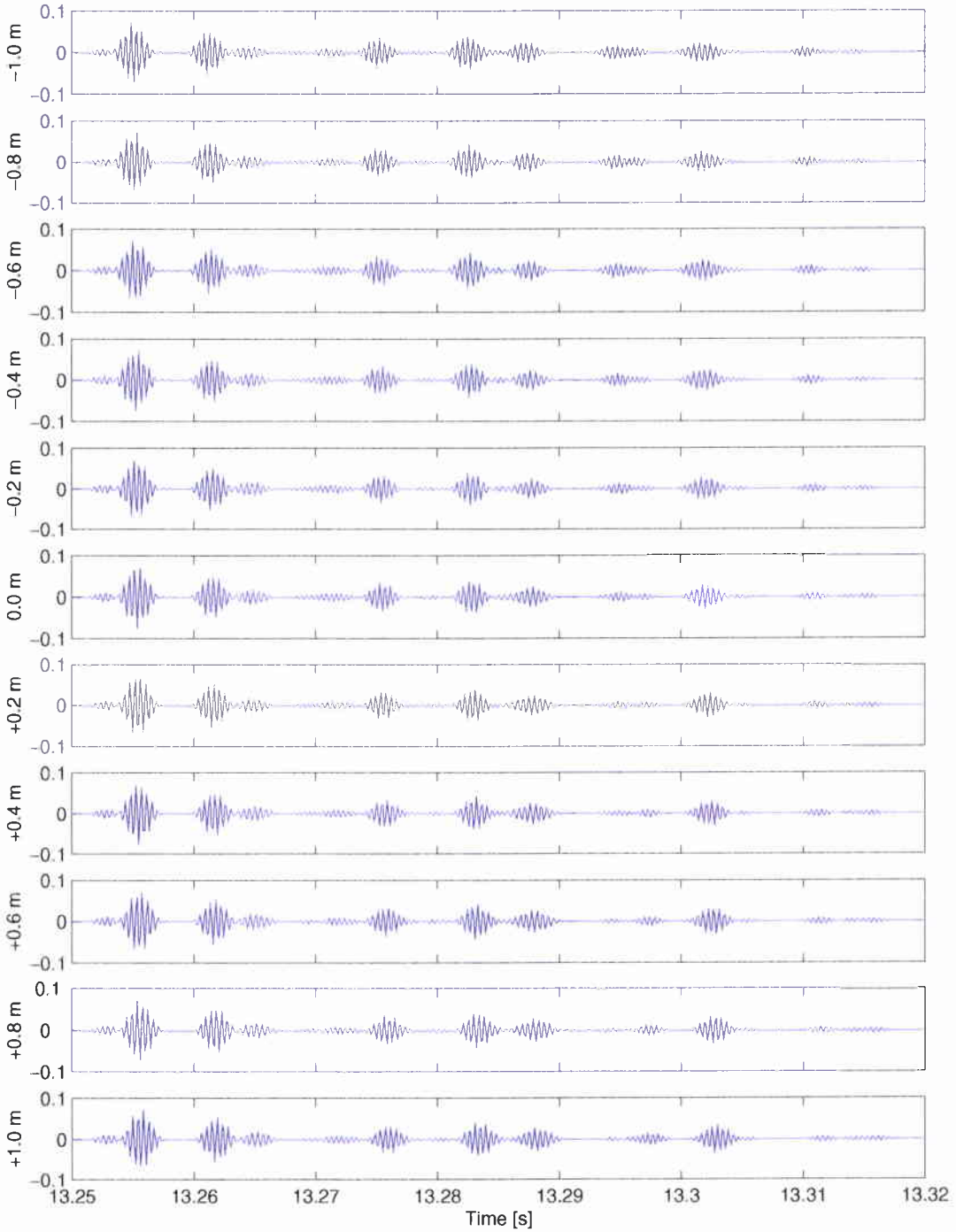

Figure 10 *Impulse responses at a range of 20 km at various bottom angles.*

The original water depth is 120 m and the bottom slope is then gradually changed: over a distance of 20 km the depth changes linearly by maximal ±1 m corresponding to an angle of $\pm 2.86 \cdot 10^{-3}$ degrees[3].
The magnitude of the complex correlation coefficient is shown in Fig. 9. Like in the previous example, a relatively fast decay of the correlation coefficient can be observed when the bottom angle is changed indicating the sensitivity of this parameter.

The explanation is that like in the previous example different portions of the impulse response are subject to different delays which can be observed in Fig. 10. There, the graphs of the impulse response are shown for a linear decrease (minus sign) and increase (plus sign) of the water column over a range of 20 km.
A linear increase (or decrease) of one meter of the water depth is equivalent to an overall increase (or decrease) of the water column by half a meter in the mean. Thus, comparing the results shown in Figures 7 and 9 we can conclude that Cases 4 and 5 are consistent.

[3]The value -1 m corresponds to a water depth of 119 m at 20 km range.

4

Conclusion

The aim of our examination was to study the effects of changes in the source-receiver geometry and in bathymetry on the impulse response of an underwater acoustic channel. The simulations confirm that the correlation between two impulse responses belonging to changed environmental parameters is a valid measure for similarities between them.
In a first experiment the classical correlation coefficient was used to measure the similarity between impulse responses resulting from different receiver depths. The results give, for example, limits to the distance between adjacent sensors of a vertical array such that the impulse responses from a source to those sensors show enough similarity to allow for conventional delay-and-sum beam forming operations on the vertical array. In a second experiment the source-receiver distance is varied. In this case the classical correlation coefficient is highly sensitive to a mere time delay between the impulse responses.
If such a time delay is not important for the specific application or if it can be compensated for then the maximal amplitude of the cross-correlation function between the two base-band equivalents of the impulse responses can be used as a measure for similarity. This correlator was then applied to the scenario of changing source-receiver distance. The results show high correlation between the impulse responses over a large range of distance variation Δ(Range) which indicates that time delay is the major reason for a decrease of the correlation coefficient. The correlator approach (instead of calculating the mere correlation coefficient) was also applied to two scenarios in which the water depths and the bottom slope were varied. The results showed a faster decrease of the maxima of the cross-correlation functions than in the previous example. The reason for this behavior is that different portions of the signal were delayed differently so that less cross-energy is added up in the correlation. Beside that, the results demonstrate that these parameters have a higher influence on impulse response variations than a change in source-receiver distance.

In the following some suggestions for further work shall be discussed. So far, all simulations were performed neglecting such effects as ambient noise, surface movement, internal waves, etc., which will reduce the achieved performance. Therefore, these effects should be included in further simulations.
Another problem may arise with the interpretation of the results if the source-receiver geometry is changing continuously. If, for example, the source and/or the receiver are mounted on moving platforms then due to the Doppler effect the corre-

lation coefficients and maxima of the cross-correlation function will also be a function of the range rate. In this case it would e.g. be important to know how fast the platforms can move through the varying environment before adaptive channel equalization algorithms stop converging. Depending on the required information bandwidth any adaptive equalization algorithms will require a minimum "learning time" and channel equalization will not be possible beyond a certain rate of change of the impulse responses. An extension of the simulations described above to include the Doppler-effect would, therefore, be of high interest. This would, however, also require substantial efforts to provide a suitable sound propagation model that would allow to simulate signal fluctuations, i.e. time variability.
And finally it should be emphasized that the simulation results should be validated with real data confirming the significance of the proposed methods for quantifying the similarity between impulse responses of gradually changing UW acoustic communication channels.

5 Acknowledgements

This study was completed under the support of the Summer Research Assistant Programme. I wish to thank the Centre for providing me the opportunity to participate in this programm.
I would like to thank my advisor Dr. Jochen Ziegenbein for introducing me to the topic and for fruitful discussions while working on some problems. Furthermore, I am greatly indebted to Dr. Peter Nielsen for sharing his wisdom on correlation of time series with me as well as for his immense patience in answering my questions.

References

[1] A. Baggeroer, W.A. Kuperman and P. Mikhalevsky, An Overview on Matched Field Methods in Ocean Acoustics, *IEEE Journal of Oceanic Engineering* , Vol. 18, No. 4, pp. 401-424, October 1993

[2] N. Bleistein, *Mathematical Methods for Wave Phenomena*, Academic Press, Orlando, 1984

[3] I.N. Bronstein and K.A. Semendjajew, *Taschenbuch der Mathematik*, 24th edition, B.G. Teubner Verlagsgesellschaft, Leipzig, 1979

[4] C.A. Boyles, *Acoustic Waveguides: Applications to Oceanic Science*, John Wiley & Sons, New York, 1984

[5] W.S. Burdic, *Underwater Acoustic System Analysis*, Prentice-Hall, Englewood Cliffs, 1984

[6] L.M. Brekhovskikh and O.A. Godin, *Acoustics of Layered Media I: Plane and Quasi-Plane Waves*, Springer-Verlag, Berlin, 1990

[7] G.C. Carter and E.R. Robinson, Ocean Effects on Time Delay Estimation Requiring Adaptation, *IEEE Journal of Oceanic Engineering*, Vol. 18, No. 4, pp. 367-378, October 1993

[8] M.D. Collins and W.A. Kuperman, Focalization: Environmental Focusing and Source Localization, *The Journal of the Acoustical Society of America*, **90**(3), pp. 1410-1422, September 1991

[9] R.B. Evans, A Coupled Mode Solution for Acoustic Propagation in a Waveguide with Stepwise Depth Variations of a Penetrable Bottom, *The Journal of the Acoustical Society of America*, **74**(1), pp. 188-195, July 1983

[10] M. Fink, Time Reversed Acoustics, *Physics Today*, pp. 37-40, March 1997

[11] J.C. Hassab, *Underwater Signal and Data Processing*, 3rd edition, CRC Press, Boca Raton, 1989

[12] S. Haykin, *Adaptive Filter Theory*, Prentice-Hall, Upper Saddle River, 1996

[13] F.B. Jensen, W.A. Kuperman, M.B. Porter and H. Schmidt, *Computational Ocean Acoustics*, AIP Press, Woodbury, 1993

[14] L.D. Landau and E.M. Lifshitz, *Fluid Mechanics*, 2nd edition, Pergamon Press, Oxford, 1987

[15] R.O. Nielsen, *Sonar Signal Processing*, Artech House, Boston, 1991

[16] J.G. Proakis, *Digital Communications*, 3rd edition, McGraw-Hill, Boston, 1995

[17] R.A. Roberts and C.T. Mullis, *Digital Signal Processing*, Addison-Wesley, Reading, 1987

[18] H.W. Schüßler, *Netzwerke, Signale und Systeme 2*, 3rd edition, Springer-Verlag, Berlin, 1991

[19] D.G. Simons, R.A. v.d. Roer, *User Manual of the PROSIM Software Package*, TNO Physics and Electronics Laboratory, The Hague, 1999

[20] A. Sommerfeld, *Partielle Differentialgleichungen der Physik*, Dieterich'sche Verlagsbuchhandlung, Wiesbaden, 1947

[21] H.C. Song, W.A. Kuperman, W.S. Hodgkis, T. Akal and C. Ferla, Iterative Time Reversal in the Ocean, *The Journal of the Acoustical Society of America*, **105**(6), pp. 3176-3184, June 1999

[22] A. Tolstoy, *Matched Field Processing For Underwater Acoustics*, World Scientific Pub, Singapure, 1993

[23] D.E. Vakman, *Sophisticated Signals and the Uncertainty Principle in Radar*, Springer-Verlag, New York, 1968

[24] A.D. Waite, *Sonar For Practising Engineers*, 2nd Edition, Thomson Marconi Sonar Limited, Stockport, 1998

Annex A

Complex Baseband Representation of Signals

A1 Complex Baseband Representation

In many applications one encounters bandpass signals which are centered around a carrier frequency f_c. To obtain a unified treatment of these signals independent of f_c the *complex baseband representation* of signals is introduced.
Let us denote with $p(t)$ the original real-valued bandpass signal. Then, as an intermediate step, the *analytical signal*

$$p^+(t) = p(t) + j\mathcal{H}\{p(t)\}$$

can be computed using the *Hilbert transform*

$$\mathcal{H}\{p(t)\} = p(t) * \frac{1}{\pi\, t}\,.$$

For positive frequencies the spectrum of $p^+(t)$ is twice the spectrum of $p(t)$ but it is zero for negative frequencies. As the spectrum of the real bandpass signal is symmetric there is no information loss in suppressing the negative frequency content but $p^+(t)$ is a complex signal.
Shifting the remaining positive frequency content of $p^+(t)$ centered around f_c down to zero and considering a factor of $1/\sqrt{2}$ to obtain the same energy content as in $p(t)$ we get the *complex baseband representation*

$$\tilde{p}(t) = \frac{1}{\sqrt{2}}\, p^+(t)\, \mathrm{e}^{-j2\pi f_c t}\,.$$

In the special case that the spectrum of the analytic signal was symmetric with respect to the frequency f_c the resulting baseband signal is a real-valued signal. The magnitude $|\tilde{p}(t)|$ of the complex baseband signal is called the *envelope* of $p(t)$.
The original bandpass signal is obtained via the inverse transformation which is given by

$$p(t) = \sqrt{2}\,\mathrm{Re}\{\tilde{p}(t)\, \mathrm{e}^{j2\pi f_c t}\}\,.$$

A2 Correlation of Complex Baseband Signals

Let

$$p_1(t) \;=\; \sqrt{2}\,\mathrm{Re}\{\tilde{p}_1(t)\, \mathrm{e}^{j2\pi f_c t}\} = \frac{1}{\sqrt{2}}\left[\tilde{p}_1(t)\, \mathrm{e}^{j2\pi f_c t} + \tilde{p}_1^*(t)\, \mathrm{e}^{-j2\pi f_c t}\right]$$

$$p_2(t) \;=\; \sqrt{2}\,\mathrm{Re}\{\tilde{p}_2(t)\,\mathrm{e}^{j2\pi f_c t}\} = \frac{1}{\sqrt{2}}\left[\tilde{p}_2(t)\,\mathrm{e}^{j2\pi f_c t} + \tilde{p}_2^*(t)\,\mathrm{e}^{-j2\pi f_c t}\right]$$

be two bandpass signals and $\tilde{p}_1(t)$ and $\tilde{p}_2(t)$ their respective baseband equivalents. Then, we can express the cross-correlation function between the two bandpass signals in terms of the equivalent baseband signals like follows:

$$\begin{aligned}
&\int_{-\infty}^{\infty} p_1(t)\;[p_2(t-\tau)]^*\;\mathrm{d}t = \\
&= \frac{1}{2}\int_{-\infty}^{\infty}\left[\tilde{p}_1(t)\,\mathrm{e}^{j2\pi f_c t} + \tilde{p}_1^*(t)\,\mathrm{e}^{-j2\pi f_c t}\right] \\
&\qquad \cdot\left[\tilde{p}_2(t-\tau)\,\mathrm{e}^{j2\pi f_c(t-\tau} + \tilde{p}_2^*(t-\tau)\,\mathrm{e}^{-j2\pi f_c(t-\tau)}\right]\,\mathrm{d}t \\
&= \frac{1}{2}\,\mathrm{e}^{-j2\pi f_c\tau}\int_{-\infty}^{\infty}\tilde{p}_1(t)\,\tilde{p}_2(t-\tau)\,\mathrm{e}^{j2\pi(2f_c)t}\,\mathrm{d}t \\
&\quad + \frac{1}{2}\,\mathrm{e}^{j2\pi f_c\tau}\int_{-\infty}^{\infty}\tilde{p}_1(t)\,\tilde{p}_2^*(t-\tau)\,\mathrm{d}t \\
&\quad + \frac{1}{2}\,\mathrm{e}^{-j2\pi f_c\tau}\int_{-\infty}^{\infty}\tilde{p}_1^*(t)\,\tilde{p}_2(t-\tau)\,\mathrm{d}t \\
&\quad + \frac{1}{2}\,\mathrm{e}^{j2\pi f_c\tau}\int_{-\infty}^{\infty}\tilde{p}_1^*(t)\,\tilde{p}_2^*(t-\tau)\,\mathrm{e}^{-j2\pi(2f_c)t}\,\mathrm{d}t \qquad (12)\\
&= \mathrm{Re}\left\{e^{j2\pi f_c\tau}\,\tilde{p}_1(\tau) * \tilde{p}_2^*(-\tau)\right\} \qquad (13)
\end{aligned}$$

The first and the last term in (12) are the value of the spectrum $\tilde{p}_1(\omega)\tilde{p}_2^*(\omega)$ at $\omega = \pm 2\pi(2f_c)$. As $\tilde{p}_1(\omega)$ and $\tilde{p}_2(\omega)$ are non-zero only in the frequency range $[-2\pi f_c;\, 2\pi f_c]$ - otherwise the original signals $p_1(t)$ and $p_2(t)$ would not be bandpass signals centered around f_c - the two integrals are zero.
It can be further seen from equation (13) that the cross-correlation of the two bandpass signals is again a bandpass signal centered around f_c.

Additionally, we prove that the maximum magnitude of the baseband cross-correlation function $\tilde{R}_{12}(\tau)$ is an upper bound of the maximum magnitude of $\tilde{R}_{12}(\tau)$:

$$\begin{aligned}
\max_\tau |R_{12}(\tau)| \;&=\; \max_\tau \left|\mathrm{Re}\left\{\mathrm{e}^{j2\pi f_c\tau}\,\tilde{R}_{12}(\tau)\right\}\right| \\
&= \frac{1}{2}\max_\tau \left|\tilde{R}_{12}(\tau)\,\mathrm{e}^{j2\pi f_c\tau} + \tilde{R}_{12}^*(\tau)\,\mathrm{e}^{-j2\pi f_c\tau}\right| \\
&\le \frac{1}{2}\max_\tau \left\{\left|\tilde{R}_{12}(\tau)\right| + \left|\tilde{R}_{12}^*(\tau)\right|\right\}
\end{aligned}$$

$$= \max_{\tau} \left| \tilde{R}_{12}(\tau) \right| .$$

Thus, the complex correlation coefficient as defined in equation (11) is always an upper bound of the correlation coefficient as given in equation (10).

Document Data Sheet

Security Classification		Project No.
UNCLASSIFIED		04-A
Document Serial No.	**Date of Issue**	**Total Pages**
SM-373	April 2000	34 pp.

Author(s)

Weber, R.

Title

On the spatial variability of the impulse response of an underwater acoustic channel

Abstract

In many applications like adaptive equalization, beam-forming, matched field processing or focalization the performance is limited due to changes in the impulse response caused by variations in source-receiver range or in bathymetry. As one wishes to quantify the degree of degradation and possibly compensate them it is important to understand the effects of parameter variations on the impulse response.

This report focuses on examining the similarities of simulated impulse responses belonging to scenarios in which environmental parameters are changed one at a time. As a measure of similarity the classical correlation coefficient and the maximum magnitude of the cross correlation function between the complex equivalent lowpass representation of the signals are introduced and their properties are discussed. The results of the correlation analysis demonstrate the properties of the two correlators and show the limits of their applicability. Furthermore, they give evidence that some parameter perturbations are more critical for impulse response variations than others.

Keywords

Issuing Organization

North Atlantic Treaty Organization
SACLANT Undersea Research Centre
Viale San Bartolomeo 400, 19138 La Spezia, Italy

[From N. America: SACLANTCEN (New York) APO AE 09613]

Tel: +39 0187 527 361
Fax:+39 0187 527 700

E-mail: library@saclantc.nato.int

The SACLANT Undersea Research Centre provides the Supreme Allied Commander Atlantic (SACLANT) with scientific and technical assistance under the terms of its NATO charter, which entered into force on 1 February 1963. Without prejudice to this main task - and under the policy direction of SACLANT - the Centre also renders scientific and technical assistance to the individual NATO nations.

SACLANT Undersea Research Centre
Viale San Bartolomeo 400
19138 San Bartolomeo (SP), Italy

tel: +39 0187 527 (1) or extension
fax: +39 0187 527 700

e-mail: library@saclantc.nato.int

NORTH ATLANTIC TREATY ORGANIZATION